Journal of the Brazilian Society of Mechanical Sciences and Engineering (2021) 43:356
https://doi.org/10.1007/s40430-021-03036-y

TECHNICAL PAPER

Friction and wear characteristics of linear contact sliding friction pairs under oil-air lubrication

Xiangyu Xie[1] · Zhaoyang Zeng[2] · Jun Luo[1] · Jin Xu[2]

Received: 3 December 2020 / Accepted: 15 May 2021 / Published online: 21 June 2021

Abstract
Oil-air lubrication has been extensively used in mechanical equipment fields. The study aimed to evaluate the tribological behavior of linear contact sliding friction pairs under oil-air lubrication. An oil-air lubrication equipment was developed, and linear contact sliding friction under oil-air lubrication test was carried out on a reciprocating wear test device. Microscopic feature and composition distribution of the wear scars were conducted using scanning electron microscopy, optical white-light interferometer, energy-dispersive X-ray spectroscopy and Raman spectrometer. The influence rule of oil supply, oil pressure, airspeed, air pressure and oil temperature on the tribological behavior of linear contact sliding friction pairs was obtained. Experimental results demonstrate that the friction coefficient curves of different parameters are composed of four stages, namely, the initial stage, the recede stage, the ascent stage and the stable stage. The relationship between oil-air lubrication test parameters and wear was discussed. The wear mechanisms of linear contact sliding friction pairs under oil-air lubrication are delamination wear, abrasive wear and oxidation wear.

Keywords Friction coefficient · Oil-air lubrication · Linear contact sliding · Wear mechanism

1 Introduction

Oil-air lubrication which delivers the lubricating oil to the lubricating point has been applied commonly because of its accuracy in oil quantity control and high cooling efficiency with high-speed compressed air. With excellent advantages such as high-efficient lubrication, energy conservation and environmental protection, oil-air lubrication has been extensively used in mechanical equipment fields such as numerical control machine tool, high-speed train wheels and rails, and aeroengines [1–3]. In recent years, many studies have focused on the tribological performance under oil-air lubrication. Wu et al. [4] studied the thermal deformation and the static stiffness of an oil-air lubricated spindle and established the optimal operating conditions for the smallest temperature increase. Hohn et al. [5] investigated the limits concerning possible reduction of lubricant quantity in gears without detrimental influence on the load-carrying capacity, the results showed the application potential of oil-air lubrication also for heavy duty transmissions nevertheless there exists a natural limitation for lowering the oil quantity in transmissions. Yan et al. [6, 7] studied the effect of different air supply modes on the flow performance of high-speed low-friction ball bearings, finding that the temperature between friction pairs was relatively low under the inner ring air supply mode; and applied flow visualization techniques to simulation and experiment, in order to clarify the internal flow characteristics of oil-air lubrication for high-speed ball bearing. Liu et al. [8] explored the influence of air velocity on the friction and wear characteristics of point contact sliding by carrying out friction test and numerical simulation under oil-air lubrication conditions. Tian et al. [9] calculated the effects of oil-air lubrication parameters on the friction loss

Technical Editor Monica Carvalho.

Xiangyu Xie and Zhaoyang Zeng contribute equally to this work.

✉ Jun Luo
luojun_gyu@sina.com

✉ Jin Xu
jinxu618@163.com

[1] Guizhou Provincial College-Based Engineering Research Center for Materials Protection of Wear and Corrosion, College of Chemistry and Materials Engineering, Guiyang University, Guiyang 550005, China

[2] School of Mechanical Engineering, Guizhou University, Guiyang 550000, China

of angular contact ball bearing and performed an experiment to derive the empirical formula with respect to the lubricant flow, air pressure, rotating speed, and pitch diameter. Li et al. [10] investigated the effects of air inlet flow rate on the bearing cavity and operating conditions during the oil-air lubrication, and established a corresponding rolling bearing model. Zeng et al. [11] simulated the oil-air two-phase flow for traditional oil-air lubrication unit and designed a new oil-air lubrication unit for high/ultrahigh-speed grinding machine. The optimal structure parameters for the optimum flow pattern and operating conditions for low vibration and noise were obtained.

At present, scholars have drawn a lot of meaningful conclusions on oil-air lubrication characteristics and pointed out that the influence of these characteristics is closely related to the tribological and wear behaviors between friction pairs [12]. Previous research [13] has demonstrated that in oil-air lubrication, the air supply has a great influence on spread of contact point lubricating oil, which further affects the formation of contact point oil film and finally leads to the difference in contact point friction characteristics. The effect of contact temperature [14] in oil-air lubrication would increase the ambient temperature resulted in the wear of the specimen surface in different degrees. Meanwhile, most scholars focused on point contact friction pairs and these studies are very helpful for the understanding of the wear characteristics under oil-air lubrication conditions. Linear contact sliding friction pairs under oil-air lubrication conditions are also widely used in engineering, such as roller and cage assembly, wheel shaft fit, etc. However, the study of friction characteristics of linear contact under oil-air lubrication is scarce. The possible reason is that the test device in the form of point contact is easy to realize, while the form of linear contact has some special requirements on the test device. Moreover, since it is particularly difficult to ensure the uniform load on the contact surface of friction pairs especially under the oil-air lubrication, a little error will make the test results have a great difference for linear contact, and the theory of point contact cannot explain some linear contact phenomena under oil-air lubrication [15]. This study developed an oil-air lubrication experimental device, and realized linear contact on friction pairs between roller and flat through the careful modification of the fixture, and carried out an oil-air lubrication parameter test with a wear test equipment to study the influence of oil supply, oil pressure, airspeed, air pressure and oil temperature on the tribological behavior of linear contact sliding friction pairs. The wear mechanism of linear contact friction pairs under oil-air lubrication was determined. The study results could provide reference for the design and application of mechanical equipment under oil-air lubrication.

2 Experimental procedure

2.1 Oil-air lubrication device

The test aimed to examine the effect of linear contact sliding wear characteristics on roller bearings under oil-air lubrication condition. An oil-air lubrication experimental device was designed and developed (Fig. 1). The operating process of the oil-air lubrication device is as follows: The air compressor (1) works and air is from the atmosphere in the laboratory, and the compressed air is filtered by the filter pressure reducing valve (2) and reaches the airflow meter (3). The required airflow is controlled, calculated and continuously delivered to the oil-air mixing block (5). Meanwhile, the gear pump (9) starts to work. According to the set oil supply time and cycle, the lubricating oil distributes the required lubricating oil through the oil distributor (12). The distributed lubricating oil enters the oil-air mixing block, where the oil-air mixture is sprayed to the linear contact friction pair (7) through the nozzle (6) after the compressed air and the lubricating oil are mixed. Finally, the data acquisition and control system (8) collects the data of air pressure, oil pressure and oil temperature in real time through the air pressure sensor (4), oil pressure sensor (13) and temperature sensor (11), which is fed back to the single chip for control processing in time. The single chip sends signals to specific components such as gear pump and airflow meter according to the feedback signals, thus realizing accurate oil transportation and ensuring the formation conditions of air-oil flow.

2.2 Experimental materials

The upper sample was M50 steel [16] with a size of $\Phi 12 \times 12$ mm, which was first cleaned in an ethanol ultrasonic bath for about 5 min prior to the wear test. Then, the sample was secured in an appropriate customized holder suspended to the specimen stage. Table 1 lists the chemical composition of M50 steel. The fundamental mechanical properties are described in Table 2.

The counter specimen, which was also M50 steel flat with dimensions 30 mm × 20 mm × 10 mm, the surface of all flat specimens was produced by wet grinding on 400, 800, 1200, and 2000-grit sand papers, and mechanically polished to make their surface roughness about 30 nm. All specimens were cleaned ultrasonically with acetone and dried. Then, it was secured on the reciprocating stage using a pair of rectangular holders (Fig. 1) to limit vibrations. The sample was lubricated by air and ISOVG 46 hydraulic oil. Table 3 presents the performance parameters of ISOVG 46 lubricating oil [17].

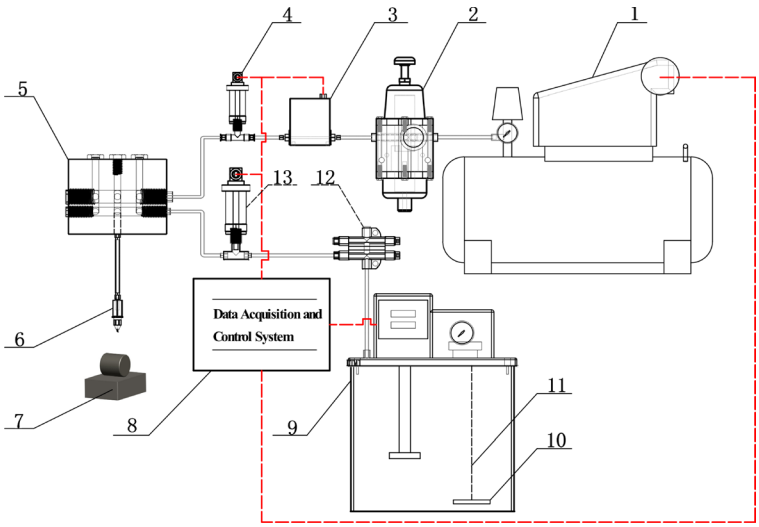

(1) air compressor, (2) filter pressure reducing valve, (3) air flowmeter, (4) air pressure sensor, (5) oil-air mixing block, (6) nozzle, (7) linear contact friction pair, (8) data acquisition and control system, (9) gear pump, (10) heating rod, (11) temperature sensor, (12) oil distributor, (13) oil pressure sensor

Fig. 1 Structure diagram of oil-air lubrication experimental device

Table 1 Elemental composition of M50 bearing steel (wt%)

Mo	Cr	V	C	Mn	Si	Ni	Fe
4.00–4.55	4.00–4.30	0.90–1.15	0.80–0.85	0.15–0.30	≤0.25	≤0.15	balance

Table 2 Main mechanical performance parameters of M50 steel

Density/ $kg.m^{-3}$	Yield strength/MPa	Modulus of elasticity/ GPa	Hardness/ HRC	Poisson ratio/*v*
7865	930	220	62.5–63	0.31

Table 3 Main parameters of ISOVG 46 hydraulic oil

kinematic viscosity(40 °C, mm^2/)	Density(kg/ m^3)	Pour point (°C)	Flash point (°C)	Surface tension (*N*/ cm)
46.12	886	− 15	195	2.75×10^{-4}

2.3 Experiment design and test details

A roller-on-flat configuration (Fig. 2) was employed to conduct an oil-air lubrication sliding wear test on a flat polished specimen using the UMT TriboLab device (Bruker, USA). With the oil-air lubrication device, the roller and flat specimen can be lubricated with a constantly flowing oil-air mixture through periodically supplied oil. The oil-air lubrication parameters are listed in Table 4.

The configuration of the UMT TriboLab device was set to the linear reciprocating configuration method. The stroke length was 1.6 mm, a constant normal load of 46 N was applied to the stationary roller, and a to-and-fro sliding velocity of the testing oscillating frequency of 0.5 Hz was used in the sample stage according to the ASTM G133 standard. The test time was 2000s, equivalent to the total number of 1000 cycles. The UMT Tribolab instrument automatically calculated and recorded the coefficient of friction (COF) with the help of electrical sensors (1000 Hz acquisition rate) using the ratio of the normal force and the horizontal frictional force. The experiment was repeated three times on each sample surface by changing the position of the roller and moving to an unworn area on the flat sample surface. The test was conducted at room temperature of 22 ± 3 °C and relative humidity of 50–60%.

Subsequent to the tribological tests, the wear scars on the samples were assessed by using a Raman spectrometer (Raman, DXRTM). The laser with wavelength of 532 nm and irradiation power of 20 mW was used. Raman spectra were collected in the range from 100 up to 2000 cm^{-1} during 10 s. Scanning electron microscopy (SEM, FEI Quanta

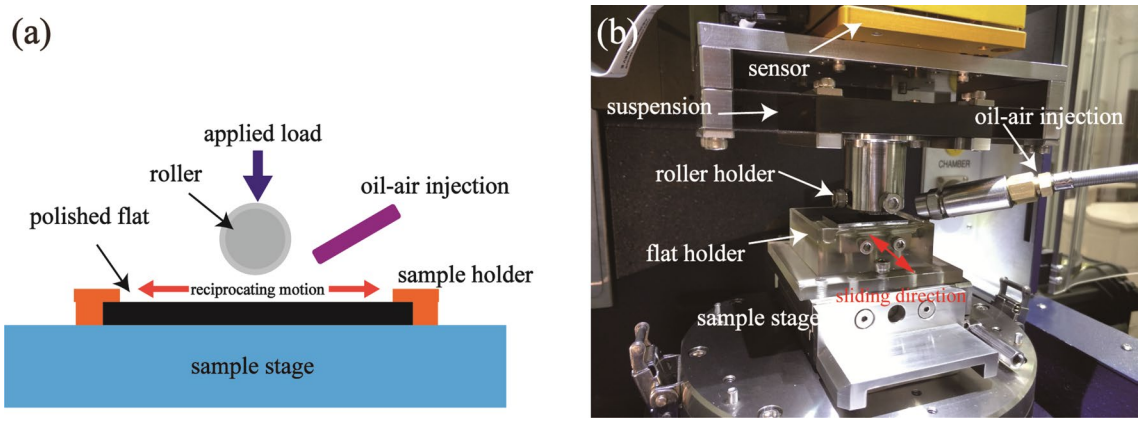

Fig. 2 Experiment of linear contact sliding friction: **a** Illustration of roller-on-flat reciprocating wear test, **b** linear contact sliding friction device under oil-air lubrication condition

Table 4 Oil-air lubrication parameters

Parameters	Oil supply q/(mL/min)	Oil pressure po/(MPa)	Airspeed v/(m/s)	Air pressure pa/(MPa)	Oil temperature T/(°C)	Injection angle θ/(°)
Value	0.1–0.6	1–2.5	1–8	0.1–0.7	24–65	30

250 FEG) and energy-dispersive X-ray spectroscopy (EDX) were employed to observe and analyze the worn flat samples, before observation, the samples were ultrasonic washed in deionized water and ethanol for 10 min, successively. The 3D topographies of the worn scars were measured by using an optical white-light interferometer (Zygo, ZeGage ™ Pro HR).

3 Results and discussion

3.1 Number of cycles

Typical oil-air lubrication condition parameters (q = 0.2 mL/min, Po = 1.5 MPa, Pa = 0.4 MPa, v = 4 m/s, T = 24 °C) were selected to carry out the friction test of the linear contact pair. The curve of friction coefficient changing with the number of cycles is shown in Fig. 3. The friction coefficient curve is composed of four stages, namely the initial stage, the recede stage, the ascent stage and the stable stage.

(1) *The initial stage* The friction coefficient fluctuates. According to the SEM morphology of the wear scars in Fig. 4a, after two cycles, some scratches occur on the surface of the wear scar in the sliding direction, but there is no obvious sliding feature. This may be because it takes some time for the lubricating oil to enter the linear contact friction pair and form an oil film.

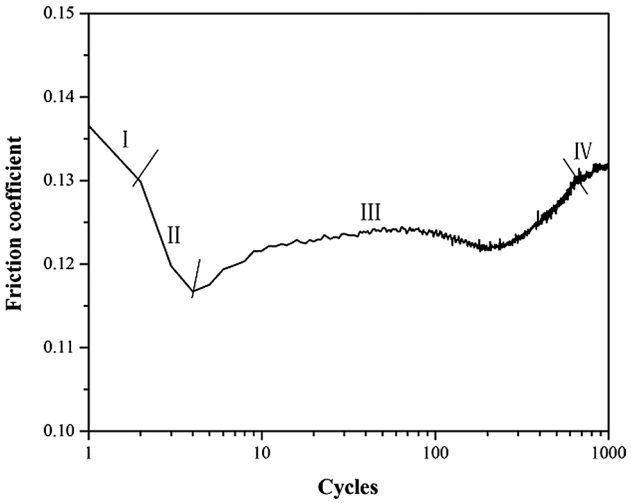

Fig. 3 Schematic diagram of friction coefficient changing with number of cycles (q = 0.2 mL/min, Po = 1.5 MPa, Pa = 0.4 MPa, v = 4 m/s, T = 24 °C)

(2) *The recede stage* The friction coefficient decreases rapidly. In Fig. 4b, the friction coefficient experiences 9 cycles, there is no obvious difference between the surface morphology of the wear scar center in the recede stage from that in the initial stage, which may be caused by the formation of a stable oil film after the lubricating oil enters the contact friction pairs.

(3) *The ascent stage* The friction coefficient curve shows an ascent trend. In the ascent stage, friction coefficient

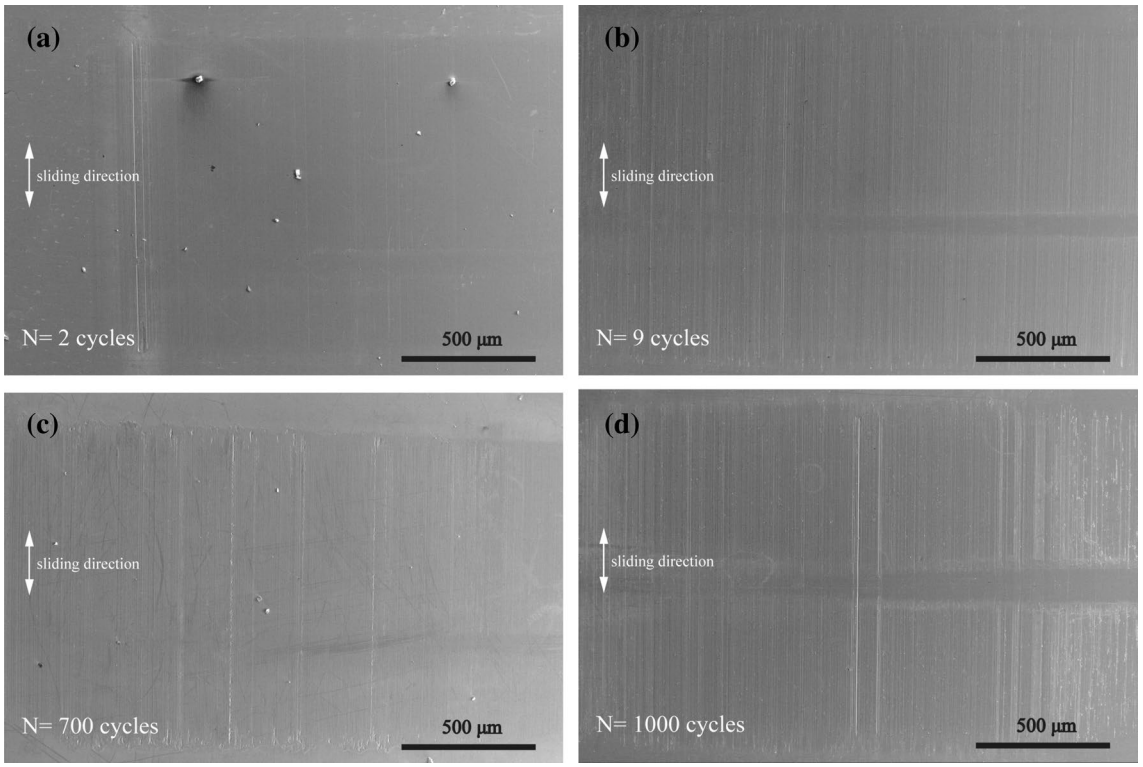

Fig. 4 Morphology of wear scars of different cycles under low-magnification SEM: **a** 2 cycles, **b** 9 cycles, **c** 700 cycles, **d** 1000 cycles

experiences about 700 cycles. According to the SEM morphology of wear scars in Fig. 4c, the area of the surface wear scars increases, and there are obvious grooves features under high magnification (Fig. 5a), pits are irregularly distributed around the grooves, the friction coefficient fluctuates.

(4) *The stable stage* The friction coefficient shows a stable trend. The friction coefficient fluctuates before stabilization. As wear debris is generated, the contact area between friction pairs will increase, which inevitably makes the friction coefficient instable. Combined with the morphology in Fig. 4d, scratches are more obvious, and grooves become deeper and denser (Fig. 5b), showing obvious linear distribution. A small number of pits appear, and the surface of wear scars shows extrusion and plastic deformation.

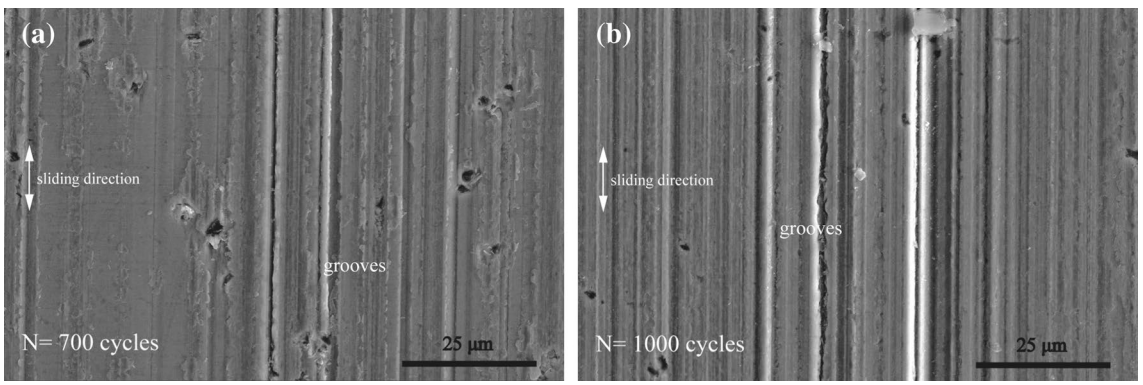

Fig. 5 Morphology of wear scars under high magnification: **a** 700 cycles, **b** 1000 cycles

3.2 Oil supply

In Fig. 6, the friction coefficient curve under different oil supply is also composed of four stages: the initial stage, the recede stage, the ascent stage and the stable stage. Under oil-air lubrication condition, the friction coefficient stabilizes when the instantaneous friction coefficient changes slightly, and sliding friction achieves stability. Therefore, the mean-steady friction coefficient is used instead of the instantaneous sliding friction coefficient. As the oil supply increases, the number of cycles needed for stable friction coefficient gradually decreases, the mean-steady friction coefficient also decreases. Particularly, when the oil supply is 0.1 mL/min, the friction coefficient fluctuates in the whole stage and keeps the largest mean-steady friction coefficient under different oil supply.

There are obvious grooves features on the wear scars surface after the oil supply test of 0.1 mL/min, which is consistent with the sliding direction. Meanwhile, there is a clear boundary between the worn area and the non-worn area (Fig. 7a). Under the oil supply of 0.2 mL/min, the peeling is not as serious as that under the oil supply of 0.1 mL/min, wear debris is accumulated on some scratches (Fig. 7b). When the oil supply is 0.4 mL/min, a large number of scratches appear on the central surface with many small peeling pits (Fig. 7c). As the oil supply increases to 0.6 mL/min, and the scratches on the central surface of the wear scars are not obvious (Fig. 7d). 3D topographies of wear marks at different oil supply are shown in Fig. 8, which shows that scratches and grooves are present across the worn surface and maximum wear depth reached 4 μm at an oil supply of 0.1 mL/min, while the worn surface seems relatively smooth at an oil supply of 0.6 mL/min. This may be because the thin lubricating oil film under low oil supply results in poor lubrication effect, indicating oil supply influences the linear contact friction significantly.

For the edge surface morphology of the wear scars under the oil supply of 0.1 mL/min, the extrusion phenomenon occurs at the edge of the wear scars, and peeling pits with different sizes appear around the grooves, which are irregularly distributed (Fig. 9a). To further investigate the composition of the surface during the sliding motion, EDS mapping analysis was adopted to determine the elemental distributions on the surface, Fe and O elements demonstrate large high-brightness area on the worn surface (Fig. 9b), and the brightness of Fe and O elements is higher on the surface of the oil supply of 0.1 mL/min than 0.6 mL/min. It can be inferred that the Fe reacted with oxygen to form the oxide film and most of the other oxides were removed during friction. A significant amount of iron and its oxide from the mating contact interfaces was adhered to worn surfaces via friction and extrusion [18, 19].

3.3 Oil pressure

To analyze the influence of oil pressure on the friction performance of linear contact, the curve of friction coefficient (as shown in Fig. 10) is also composed of four stages. As the oil pressure increases, the stabilized friction coefficient first decreases and then increases. With the increase of oil pressure, the change trend of the number of cycles needed to for the stabilization and the mean-steady friction coefficient is not obvious.

When the oil pressure is 1 MPa, the morphology of the central surface of the wear scars is mainly characterized by grooves with different sizes, which are distributed along the sliding direction, the peeling pits with different sizes are around the grooves (Fig. 11a). When the oil pressure is

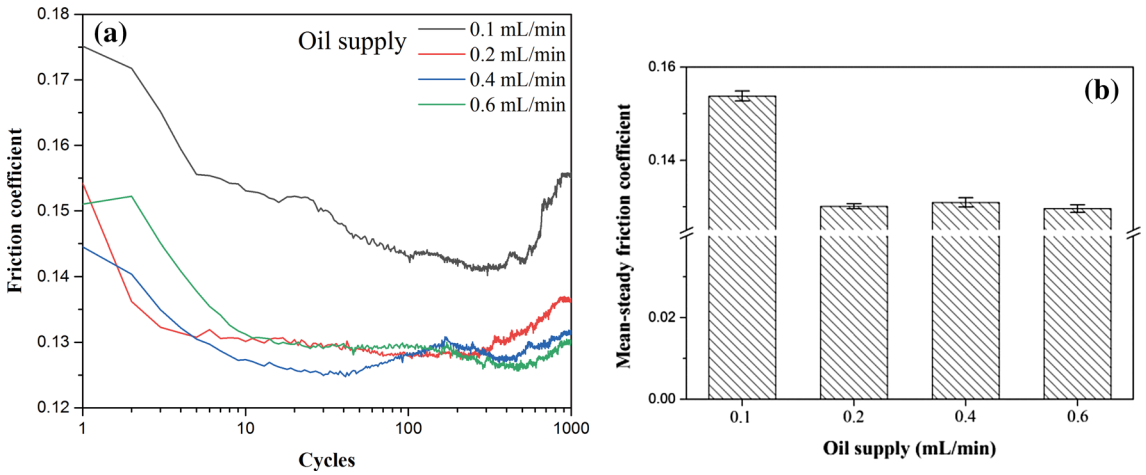

Fig. 6 Curves of friction coefficient: **a** with the number of cycles under different oil supply, **b** mean-steady friction coefficient (Po = 1.5 MPa, v = 4 m/s, Pa = 0.4 MPa, T = 24 °C)

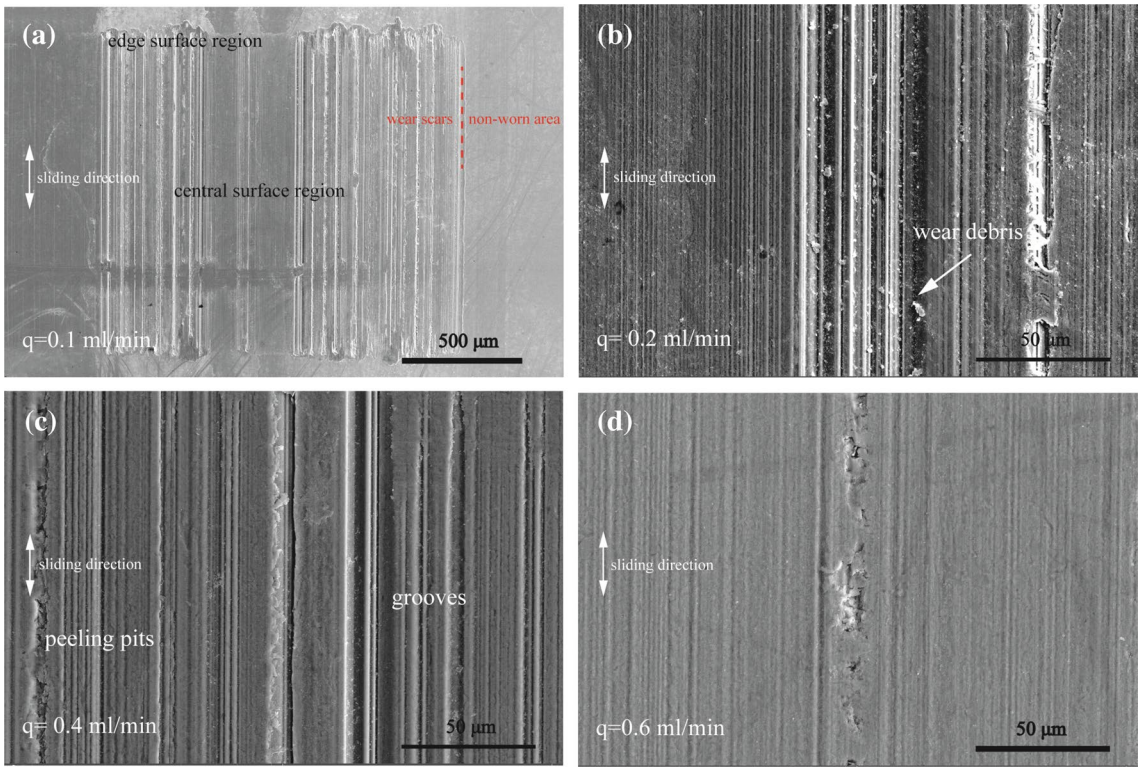

Fig. 7 Wear scars morphology: **a** at the oil supply of 0.1 mL/min, **b** central surface at the oil supply of 0.2 mL/min, **c** central surface at the oil supply of 0.4 mL/min, **d** central surface at the oil supply of 0.6 mL/min

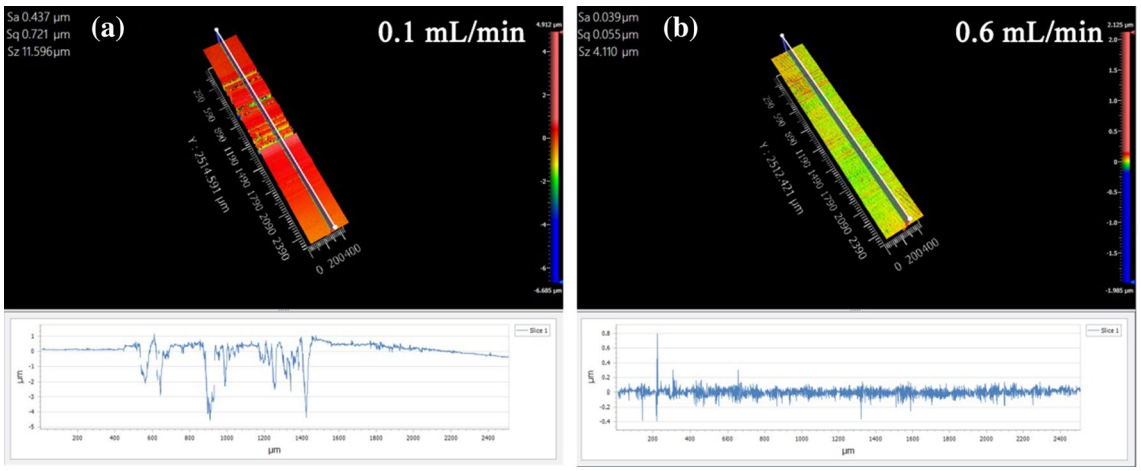

Fig. 8 3D images of wear scars and cross-profile curves on samples with: **a** the oil supply of 0.1 mL/min, **b** the oil supply of 0.6 mL/min

2 MPa, obvious grooves are formed under the action of abrasive particles (Fig. 11b). As shown in Fig. 11c, large grooves are distributed on the central surface of the wear scars at the oil pressure of 2.5 MPa, some platelet-like fragments on the sliding surfaces, the remnants of the fold are left behind as defect features on the surface, which implies delamination wear [20]. Figure 12 shows the 3D wear morphology and depth of the specimen under changing oil pressure. The depth of the wear scar increase in the case of relatively high oil pressure, the abrasive wear on the surface is more obvious.

There are plastic deformation formed by the extrusion of wear debris at the edge of the wear scars under the oil pressure of 1 MPa (Fig. 13a). It can be inferred that the

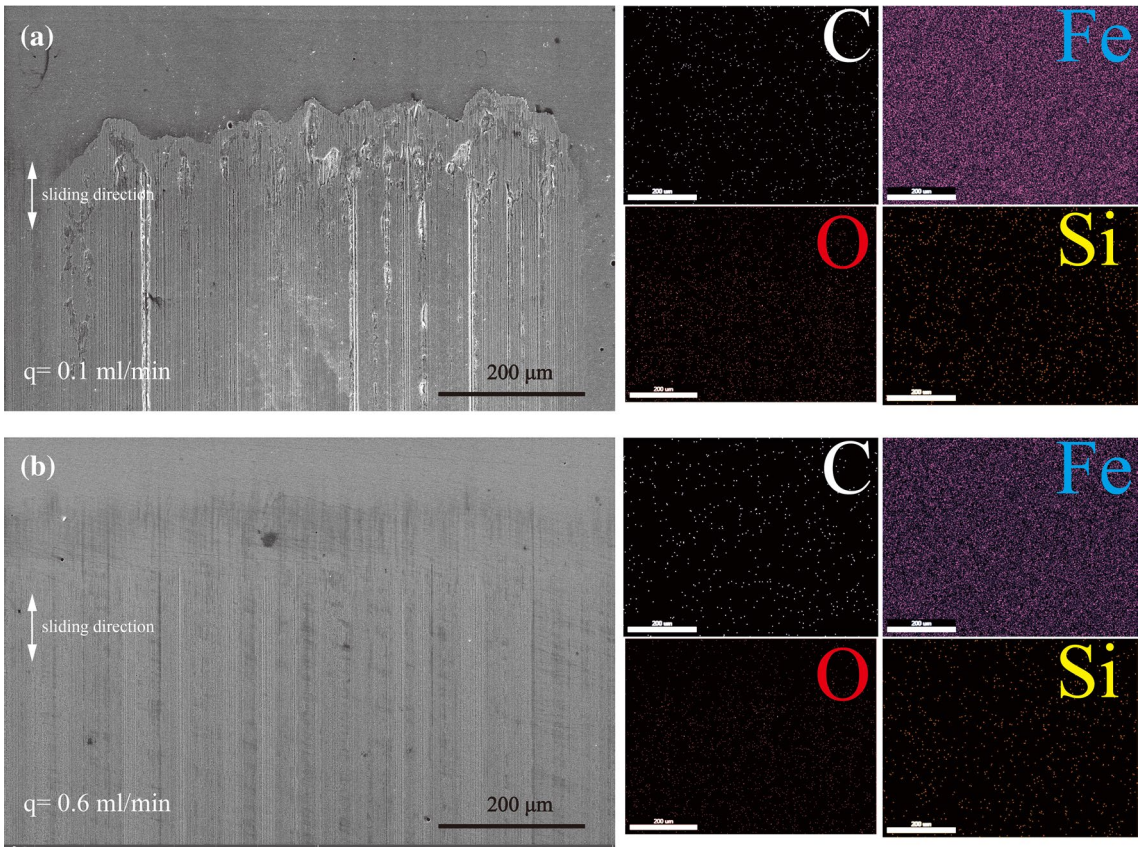

Fig. 9 SEM morphology and EDS mappings: **a** edge surface at the oil supply of 0.1 mL/min, **b** edge surface at the oil supply of 0.6 mL/min

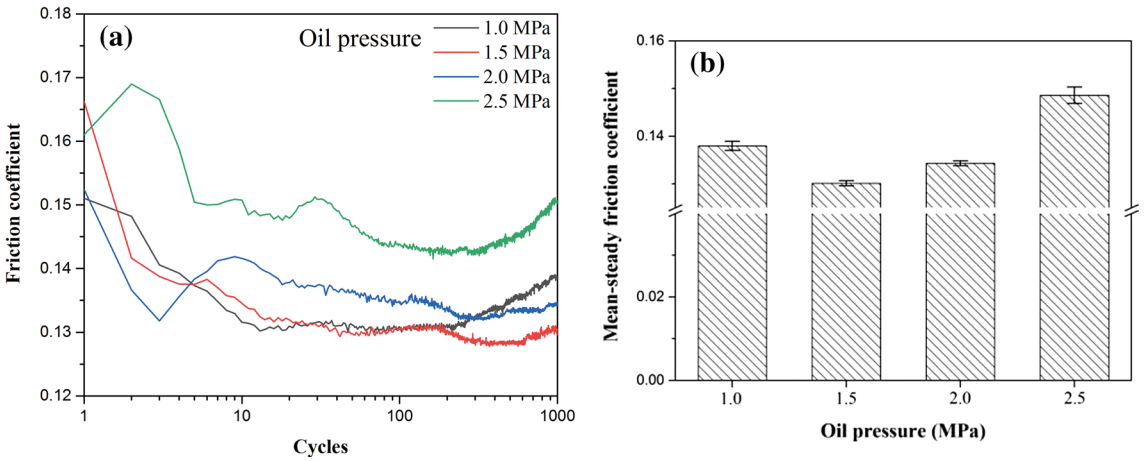

Fig. 10 Curve of friction coefficient: **a** with the number of cycles different oil pressures, **b** mean-steady friction coefficient (q = 0.2 mL/min, v = 4 m/s, Pa = 0.4 MPa, T = 24 °C)

wear debris is accumulated and continuously squeezed at the edge under the action of oil flow. EDX result shows the oxygen element peak appears on the central surface of the wear scars (Fig. 13b), also indicating oxidation wear of the linear contact pair occurs during friction. Based on the above analysis, it can be found that the overall wear is more serious under different oil pressures, and the wear mechanisms are mainly abrasive wear and delamination wear.

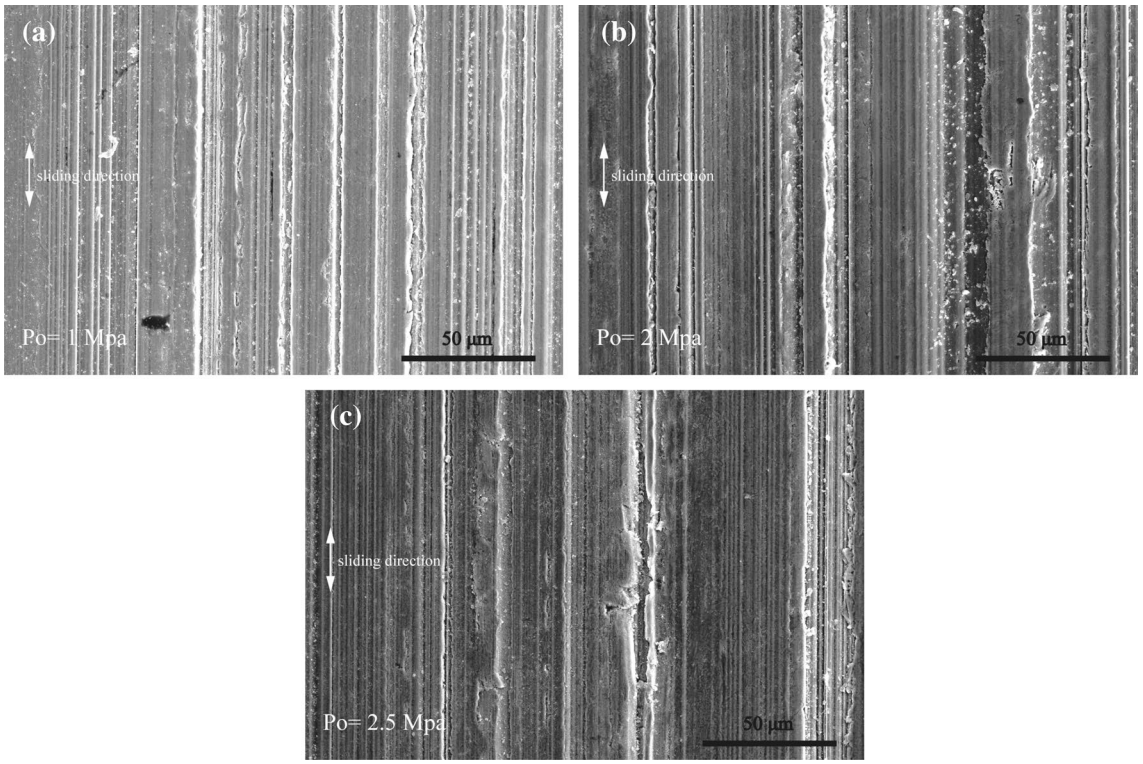

Fig. 11 SEM morphology: **a** central surface of wear scars at the oil pressure of 1 MPa, **b** central surface of wear scars at the oil pressure of 2 MPa, **c** central surface of wear scar at the oil pressure of 2.5 MPa

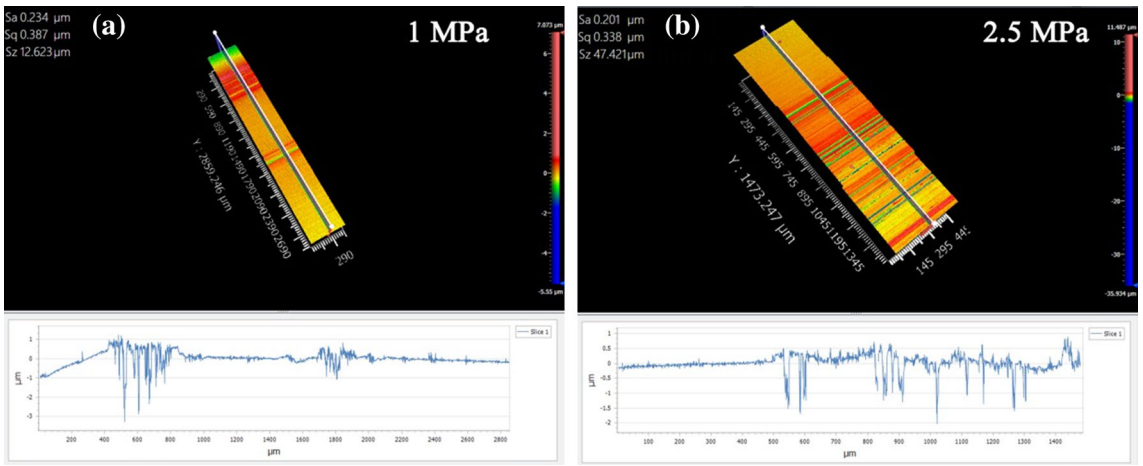

Fig. 12 3D images of wear scars and cross-profile curves on samples with: **a** the oil pressure of 1 MPa, **b** the oil pressure of 2.5 MPa

3.4 Airspeed

Figure 14 shows the curve of friction coefficient under different airspeeds, which is also compose of four stages. As airspeed increases, the mean-steady friction coefficient gradually decreases. This may be because the air supply speed directly affects the formation of a uniform and stable two-phase flow oil film for oil-air lubrication, and the high-speed airflow at a larger air supply speed can drive lubricating oil into the linear contact pair more effectively.

When the airspeed is 1 m/s, there are obvious grooves on the central surface of the wear scars along the sliding direction, large grooves are peeled off (Fig. 15a), and the abrasive debris is accumulated at the edge of the wear scars (Fig. 15b). As the airspeed increases to 2 m/s, there are obvious peeling pits with different sizes are found in

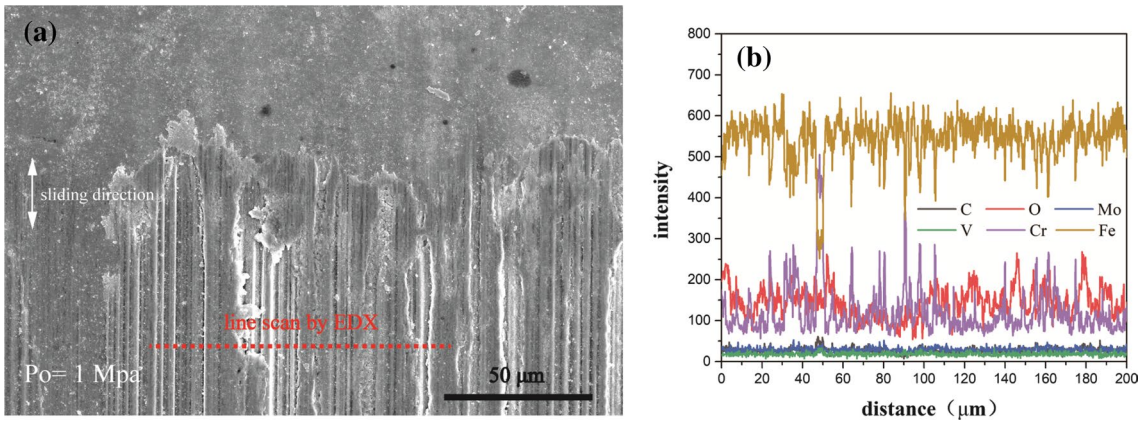

Fig. 13 Morphology of wear scars and energy spectrum at the oil pressure of 1 MPa: **a** wear scars, **b** EDX of wear scars

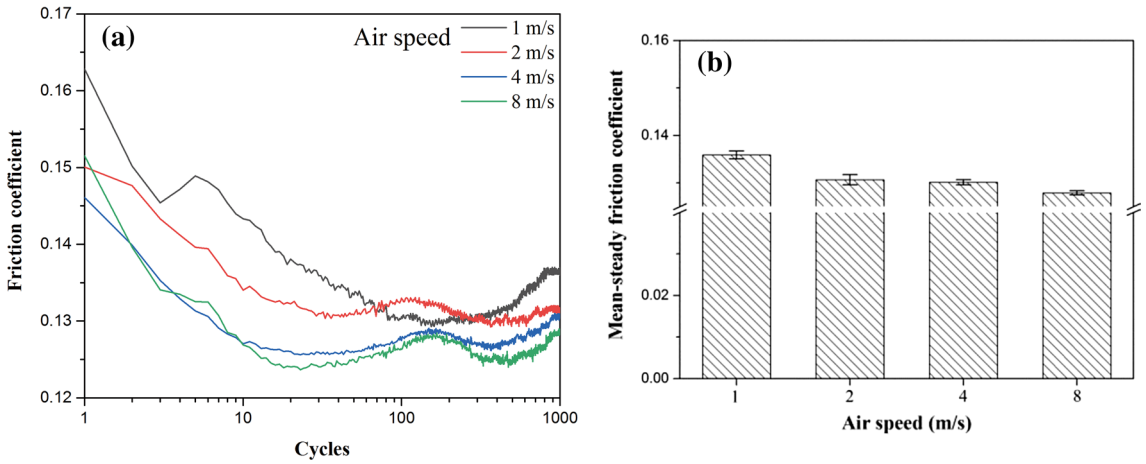

Fig. 14 Curve of friction coefficient: **a** with the number of cycles different airspeeds, **b** mean-steady friction coefficient (q = 0.2 mL/min, Po = 1.5 MPa, Pa = 0.4 MPa, T = 24 °C)

the damage area of the wear scars (Fig. 15c). The peeling layers around the peeling pits are flaky and disordered along the sliding direction, indicating that the surface of the wear scars has suffered severe three-body contact wear [21, 22]. When the airspeed is 8 m/s, the scratches have different depths and show obvious linear distribution, plastic deformation also occurs (Fig. 15d), the wear debris at the edge is obviously accumulated, and the wear of the wear scars is more serious (Fig. 15e). Figure 16 shows the surface profiles of wear scars at the airspeed of 1 m/s and 8 m/s. The wear depth of the former one was deeper than that of the latter of the sample. It was further demonstrated that increase the airspeed can effectively alleviate the wear degree of the steel surface. Further, the central surface of the wear scars at the airspeed of 1 m/s was analyzed with Raman spectrum (Fig. 17), and the products after friction oxidation on the wear scars surface contain FeO and Fe_3O_4.

3.5 Air pressure

The friction coefficient curve under different air pressures is composed of four stages. The mean-steady friction coefficient gradually decreases with the increase of air pressure (Fig. 18).

When the air pressure is 0.1 MPa, there are obvious grooves on the central surface of the wear scars (Fig. 19a), and peeling phenomenon appears around the grooves, wear debris is squeezed, deformed and accumulated, forming an obvious boundary with the non-worn area at the edge of the wear scars (Fig. 19b), profile. When the air pressure is 0.2 MPa, the grooves are uniformly distributed on the wear scars under the action of abrasive particles (Fig. 19c), the peeling phenomenon at the edge of the wear scars and the accumulation degree of wear debris decreases with the increase of air pressure, and the grooves extend to the edge (Fig. 19d). As the air pressure increases to 0.7 MPa, the wear

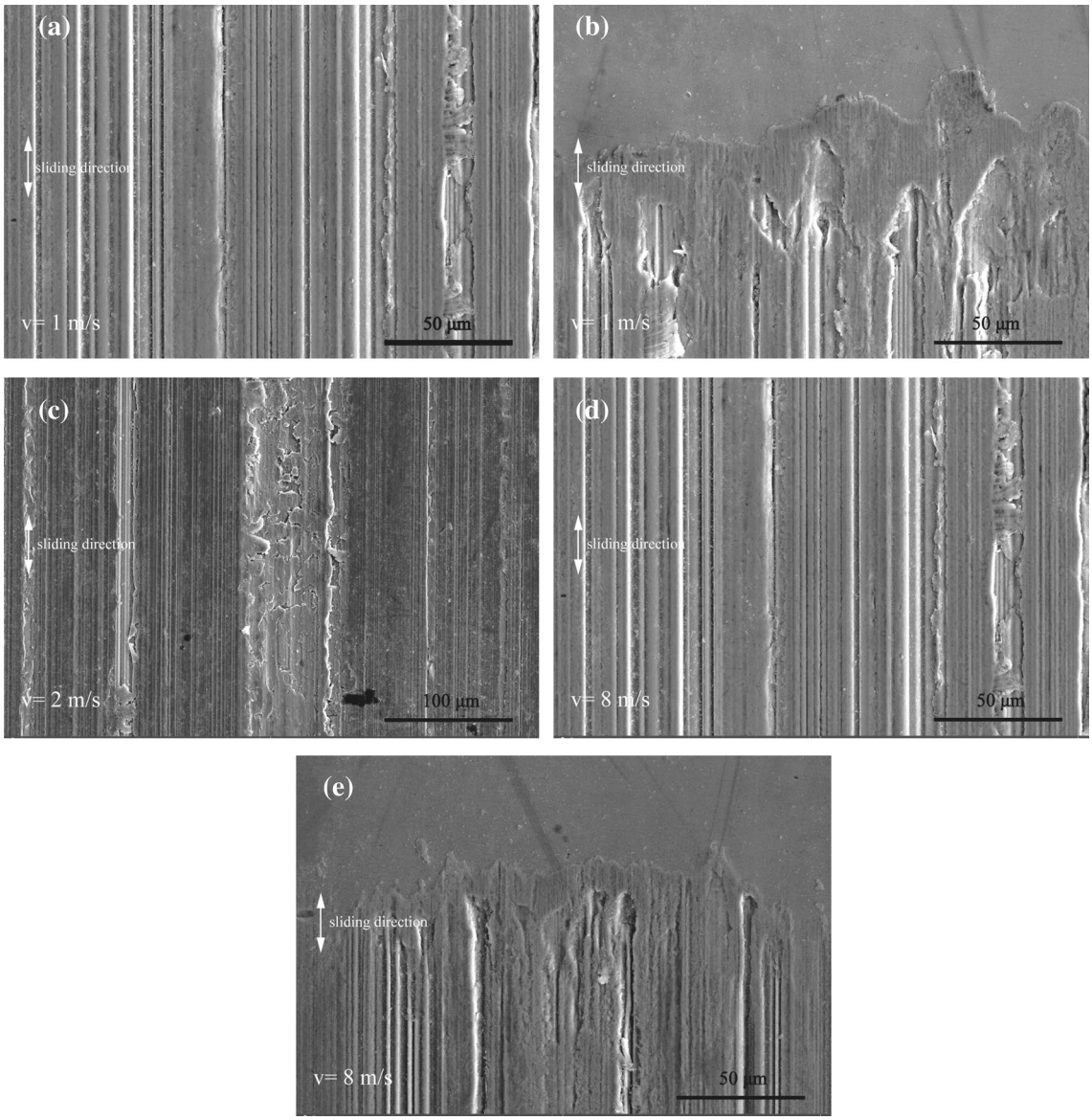

Fig. 15 SEM morphology: **a** central surface of wear scars at the airspeed of 1 m/s, **b** edge surface of wear scars at the airspeed of 1 m/s, **c** central surface of wear scars at the airspeed of 2 m/s, **d** central surface of wear scars at the airspeed of 8 m/s, **e** edge surface of wear scars at the airspeed of 8 m/s

scars are densely distributed along the sliding direction, no obvious peeling phenomenon is found on the surface of the wear scars (Fig. 19e). The shade difference of wear scars in backscattered electron (BSE) image is less significant than that of the secondary electron (SE) image at the air pressure of 0.7 MPa. However, EDS analysis indicates an oxygen element peak at the center of wear scars (Fig. 20), the wear mechanism of the sample is oxidation wear [23]. This can be judged from two reasons. The first is the shallow wear surface scratches and the oxidation feature on the wear surface, the second is the higher Fe content in the debris relative to that of other elements [24]. The main reason of the small difference between BSE and SE image may be that the amount of the oxide-based wear debris is not large enough. Figure 21 demonstrates the 3D morphologies of the wear tracks. It can be intuitively observed that the breadth of wear scar and wear volume significantly decreases with the increasing air pressure.

3.6 Oil temperature

The change curve of friction coefficient at different oil temperatures shows different trends, but it is also composed of four stages (Fig. 22). With the increase of oil temperature, the number of cycles needed for the ascent stage gradually increases, the mean-steady friction coefficient is more

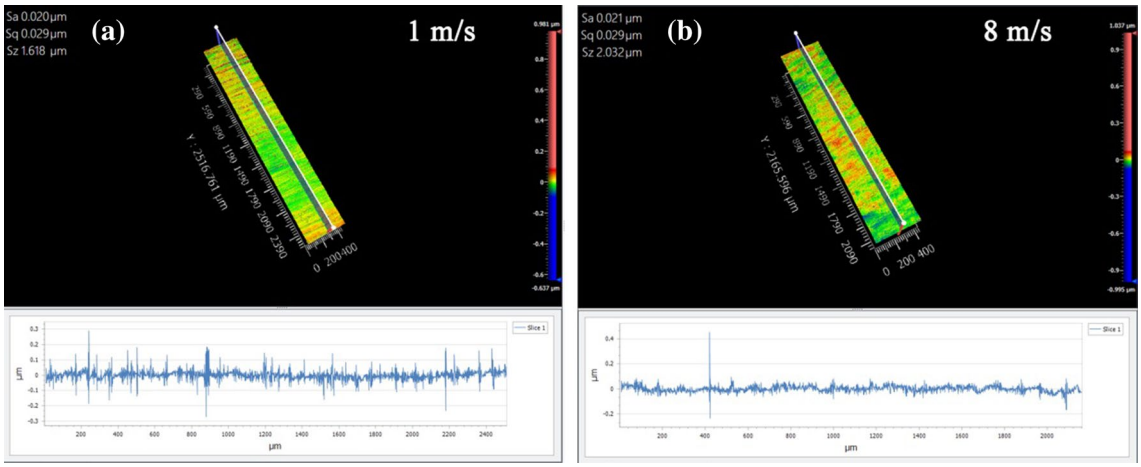

Fig. 16 3D images of wear scars and cross-profile curves on samples with: **a** the airspeed of 1 m/s, **b** the airspeed of 8 m/s

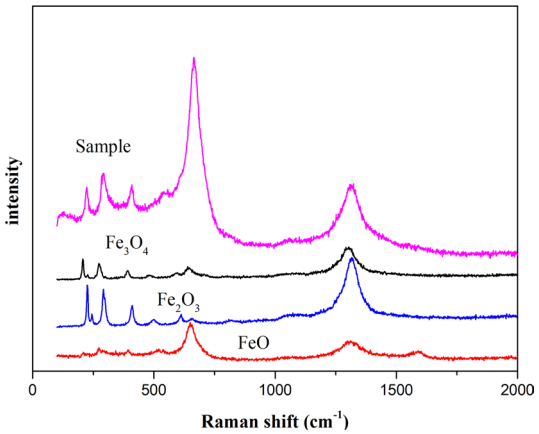

Fig. 17 Raman spectrum of central surface of wear scars at the airspeed of 1 m/s

sensitive to the changes of oil temperature than the other oil-air lubrication parameters.

At the oil temperature of 35 °C, there are grooves with different sizes along the sliding direction on the central surface of the wear scars, peeling occurs in the grooves, accompanied by plastic deformation caused by extrusion (Fig. 23a). When the oil temperature increases to 50 °C, wear contact area is larger, indicating that the wear is more serious than that at 35 °C (Figs. 23b, 24). At the oil temperature of 65 °C, more obvious grooves are caused by three-body contact under the action of abrasive particles (Fig. 23c). There are many abrasive debris in the grooves, and the peeling layers with different sizes appear. Three-body contact is caused by abrasive particles [25], resulting in serious wear on the central surface of the wear scars and accumulation of wear debris in the grooves.

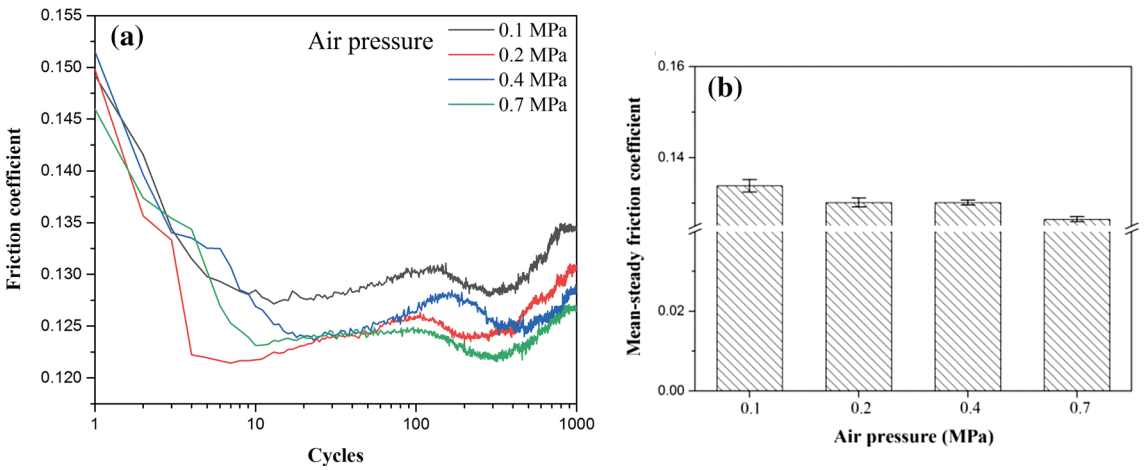

Fig. 18 Curve of friction coefficient: **a** with the number of cycles different air pressures, **b** mean-steady friction coefficient (q = 0.2 mL/min, Po = 1.5 MPa, v = 4 m/s, T = 24 °C)

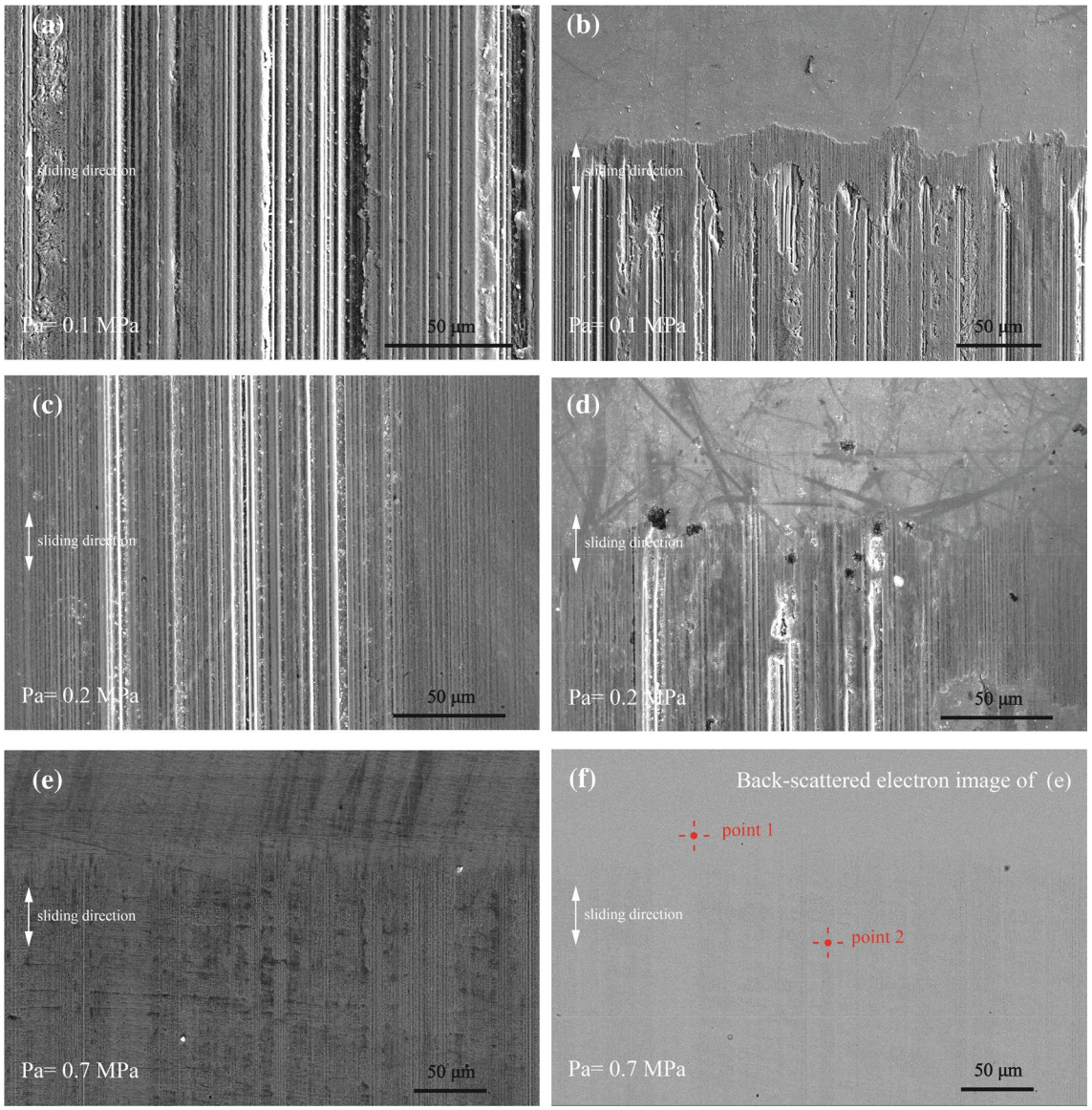

Fig. 19 SEM morphology: **a** central surface at the air pressure of 0.1 MPa, **b** edge surface at the air pressure of 0.1 MPa, **c** central surface at the air pressure of 0.2 MPa, **d** edge surface at the air pressure of 0.2 MPa, **e** central surface at the air pressure of 0.7 MPa, **f** back-scattered electron image of **e**

EDX result shows, there is oxygen element peak on the central surface of the wear scars (Fig. 25a). The central position of the wear scars was conducted with Raman spectrum analysis (Fig. 25b), the generation peak at the oil temperature of 35 °C was compared with the characteristic peak of Fe oxide standard sample, which is close to the characteristic peaks of Fe_2O_3 and Fe_3O_4. Fe_2O_3 and Fe_3O_4 are the main products on the surface of the wear scars. At relatively high or low oil temperature, the abrasive wear of scars becomes more serious and the lubrication effect is worse. This is because the viscosity of lubricating oil at about 35 °C is more conducive to the formation of oil film thickness. When the oil temperature increases to 50 °C, the viscosity of lubricating oil decreases obviously, and the oil film is unstable, making the rough peaks on the surface of linear contact pair contact directly.

4 Conclusion

This study investigated the influence of oil-air parameters such as operating cycle, oil supply, oil pressure, air supply speed, air pressure and oil temperature on the tribological behavior of linear contact sliding friction pairs by using a developed oil-air lubrication device. Moreover, the surface morphology and wear characteristics were analyzed, and the

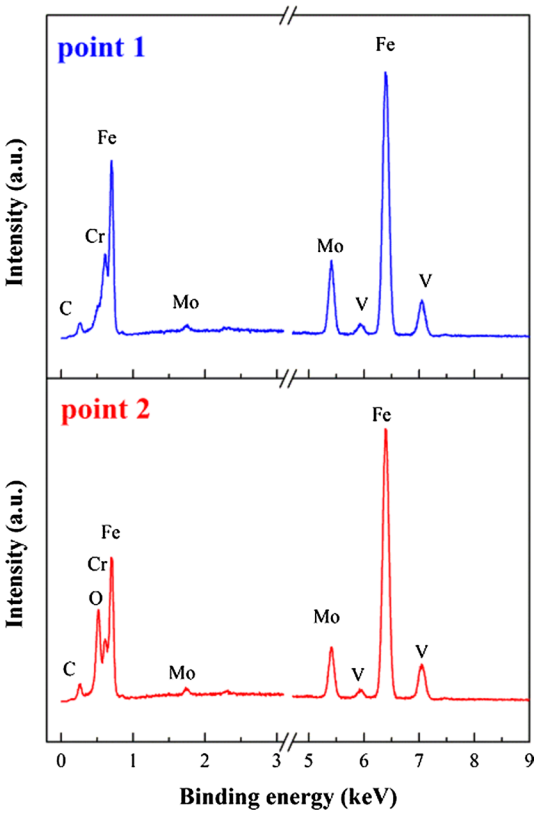

Fig. 20 Energy spectrum of wear scars at the air pressure of 0.7 MPa

wear mechanism under oil-air lubrication was revealed. The following conclusions could be drawn:

1. Under the condition of oil-air lubrication, the friction coefficient curves of different oil-air parameters are all composed of four stages, namely, the initial stage, the recede stage, the ascent stage and the stable stage. The low mean-steady friction coefficient shows the excellent lubricating property of oil-air lubrication.
2. With the increase of oil supply, the friction coefficient gradually decreases, and the number of cycles required in the stable stage also gradually decreases. The friction coefficient decreases with the acceleration of airspeed, the peeling phenomenon on the wear scars surface slows down, and the lubrication effect is gradually improved. The friction coefficient will decrease with the increase of air pressure. The coefficient of friction is more sensitive to the changes of oil temperature. With the increase of the oil pressure, the change trend of the friction coefficient is not obvious.
3. With the increase of oil supply, the grooves and peeling phenomena on the wear scars surface slow down, and the lubrication effect is gradually improved, which has obvious influence on the oil-air lubrication performance. In the case of relatively high or low oil pressure, the abrasive wear on the surface is more obvious. With the increase of air pressure or airspeed, the peeling and grooves effects on the wear scars surface decrease. At a relatively high oil temperature, the abrasive wear on the wear scars surface becomes more serious. The wear mechanisms under oil-air lubrication are delamination wear, abrasive wear and oxidation wear, and the products of oxidation wear include FeO, Fe_2O_3 and Fe_3O_4.

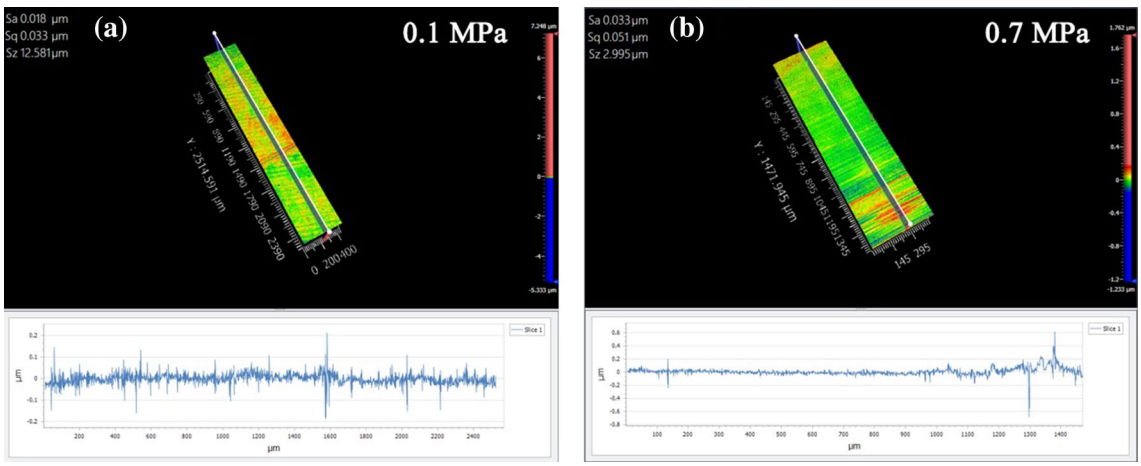

Fig. 21 3D images of wear scars and cross-profile curves on samples with: **a** the air pressure of 0.1 MPa, **b** the air pressure of 0.7 MPa

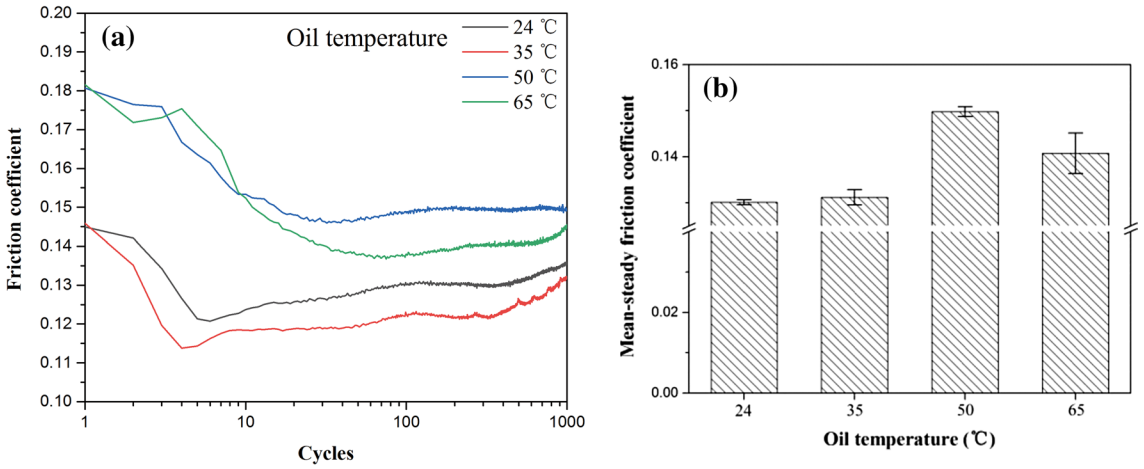

Fig. 22 Curve of friction coefficient: **a** with the number of cycles different oil temperatures, **b** mean-steady friction coefficient ($q = 0.2$ mL/min, Po = 1.5 MPa, $v = 4$ m/s, Pa = 0.4 MPa)

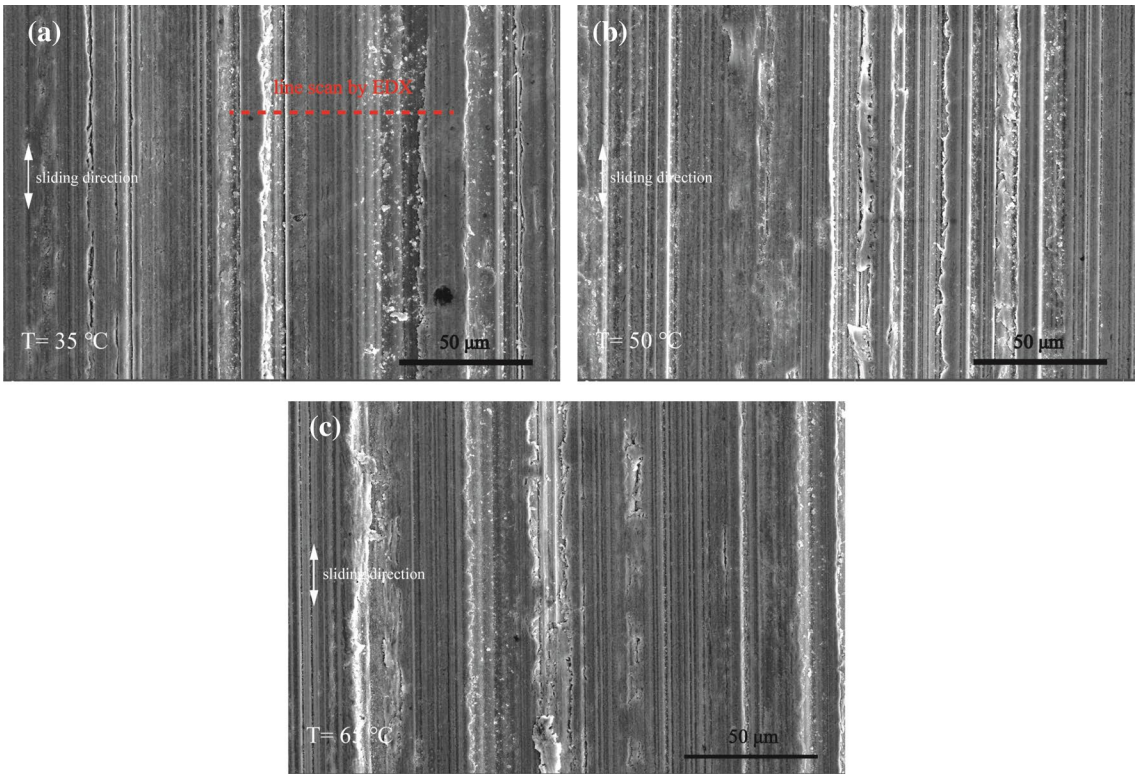

Fig. 23 SEM Morphology: **a** central surface of wear scars at oil temperature of 35 °C, **b** central surface of wear scars at oil temperature of 50 °C

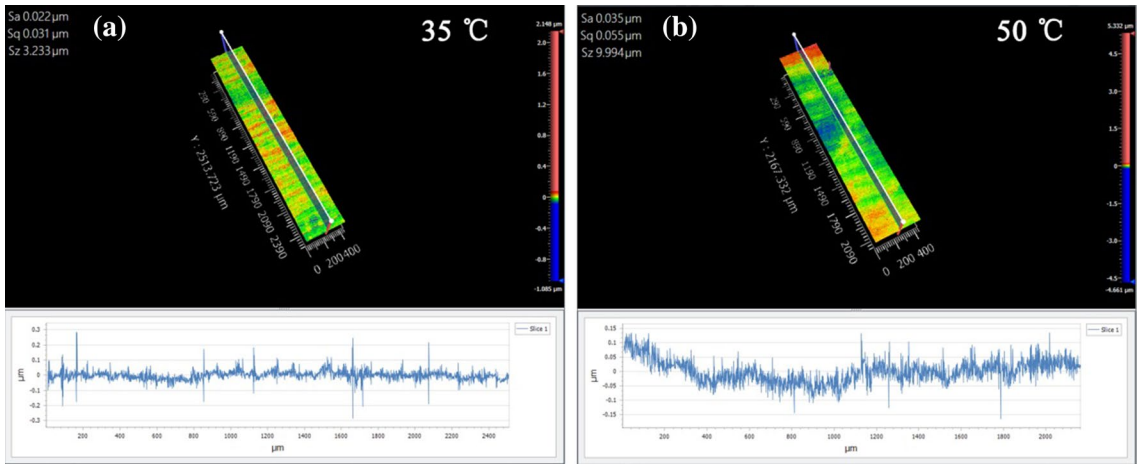

Fig. 24 3D images of wear scars and cross-profile curves on samples with: **a** oil temperature of 35 °C, **b** oil temperature of 50 °C

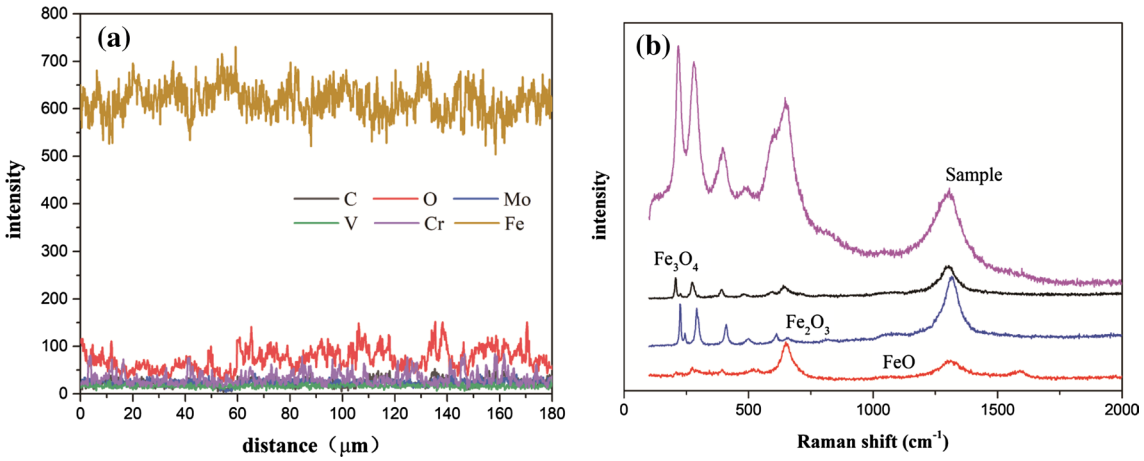

Fig. 25 Energy spectrum and Raman spectrum of wear scars at oil temperature of 35 °C

Acknowledgements The work was financially supported the National Natural Science Foundation of China (51605105), the Major Science and Technology Project in Guizhou Province (Q.K.H.Z.D.Z.X.Z [2019]3016), the Youth Science and Technology Talents Growth Fund of Education Department of Guizhou Province (KY[2018]300) and the scientific research funds of Guiyang University (GYU-KY-[2021]).

References

1. Gaca H, Ruiter J, Mehr G (2014) Oil-air systems. Springer, Berlin Heidelberg
2. Li H, Li R, Yang F, Zhang D, Zhang J (2020) Friction and wear characteristics of aluminum bronze (QAl10-4-4) bearing materials under high-temperature dry sliding conditions. J Braz Soc Mech Sci 42:354. https://doi.org/10.1007/s40430-020-02437-9
3. Jeng Y, Gao C (2001) Investigation of the ball-bearing temperature rise under an oil-air lubrication system. P I Mech Eng J-J Eng 215(2):139–148. https://doi.org/10.1243/1350650011541783
4. Wu C, Kung Y (2005) A parametric study on oil/air lubrication of a high-speed spindle. Precis Eng 29(2):162–167. https://doi.org/10.1016/j.precisioneng.2004.06.005
5. Hohn B, Michaelis K, Otto H (2009) Minimised gear lubrication by a minimum oil/air flow rate. Wear 266(3–4):461–467. https://doi.org/10.1016/j.wear.2008.04.037
6. Yan K, Dong L, Zheng J, Li B, Wang D, Sun Y (2018) Flow performance analysis of different air supply methods for high speed and low friction ball bearing. Tribol Int 121:94–107. https://doi.org/10.1016/j.triboint.2018.01.035
7. Yan K, Wang Y, Zhu Y, Hong J, Zhai Q (2016) Investigation on heat dissipation characteristic of ball bearing cage and inside cavity at ultra high rotation speed. Tribol Int 93:470–481. https://doi.org/10.1016/j.triboint.2015.09.030
8. Liu C, Tong B, Zhang G, Xu P, Wang W, Liu K (2019) Effect of air supply speed on point contact sliding wear characteristics under oil-air lubrication conditions. Lubr Sci 31(6):273–284. https://doi.org/10.1002/ls.1470
9. Tian S, Chen X, Chen T, He Y (2019) Experimental analysis and modeling of the effects of oil-air lubrication parameters on Bearings friction loss of high-speed motorized spindle. Tribol

Trans 62(3):524–534. https://doi.org/10.1080/10402004.2019.1584344
10. Li Y, Yang Z, Chen F, Zhao J (2018) Effect of air inlet flow rate on flow uniformity under oil-air lubrication. Ind Lubr Tribol 70(2):282–289. https://doi.org/10.1108/ILT-12-2016-0296
11. Zeng Q, Zhang J, Hong J, Liu C (2016) A comparative study on simulation and experiment of oil-air lubrication unit for high speed bearing. Ind Lubr Tribol 68(3):325–335. https://doi.org/10.1108/ILT-05-2015-0066
12. Liang H, Guo D, Ma L, Luo J (2015) The film forming behavior at high speeds under oil-air lubrication. Tribol Int 91:6–13. https://doi.org/10.1016/j.triboint.2015.06.010
13. Wu L, Tong B, Guo D, Ma L, Hu X (2018) Influence of oil-air lubrication flow behavior on frictional characteristics of point contact. Tribology 38(6):700–710. https://doi.org/10.16078/j.tribology.2018034
14. Liu C, Yin Y, Tong B, Zhang G (2021) Effect of oil-air lubrication on contact temperature and sliding tribological properties. Lubr Sci 33:15–28. https://doi.org/10.1002/ls.1523
15. Zhong W, Hu J, Shen P, Wang C, Lius Q (2011) Experimental investigation between rolling contact fatigue and wear of high-speed and heavy-haul railway and selection of rail material. Wear 271(9):2485–2493. https://doi.org/10.1016/j.wear.2010.12.053
16. Mukhopadhyay P, Kannaki P, Srinivas M, Roy M (2014) Microstructural developments during abrasion of m50 bearing steel. Wear 315(1–2):31–37. https://doi.org/10.1016/j.wear.2014.03.010
17. Kim S, Murrenhoff H (2012) Measurement of effective bulk modulus for hydraulic oil at low pressure. J Fluids Eng 134(2):021201. https://doi.org/10.1115/1.4005672
18. Bhushan B (1999) Principles and applications of tribology. John Wiley and Sons, USA
19. Jiang S, Mao H (2011) Investigation of the high speed rolling bearing temperature rise with oil-air lubrication. J Tribol. https://doi.org/10.1115/1.4003501
20. Mahato A, Yeung H, Guo Y, Viswanathan K, Sundaram N, Udupa A, Mann J, Chandrasekar SS (2017) Sinuous flow and folding in metals: implications for delamination wear and surface phenomena in sliding and cutting. Wear 376–377:1534–1541. https://doi.org/10.1016/j.wear.2017.02.012
21. Chang Z, Jia Q, Yuan X, Chen Y (2017) Main failure mode of oil-air lubricated rolling bearing installed in high speed machining. Tribol Int 112:68–74. https://doi.org/10.1016/j.triboint.2017.03.024
22. Kragelsky I, Alisin V (1982) Friction wear lubrication: tribology handbook. Elsevier
23. Stott F (1998) The role of oxidation in the wear of alloys. Tribol Int 31:61–71. https://doi.org/10.1016/S0301-679X(98)00008-5
24. Mishra D, Sonia F, Srivastava D, Ganesha G, Singha U, Mukhopadhyay A (2018) Wear damage and effects of graphene-based lubricants/coatings during linear reciprocating sliding wear at high contact pressure. Wear 400:144–155. https://doi.org/10.1016/j.wear.2017.12.024
25. Rus D, Capitanu L, Badita L (2014) A qualitative correlation between friction coefficient and steel surface wear in linear dry sliding contact to polymers with SGF. Friction 2(1):47–57. https://doi.org/10.1007/s40544-014-0038-2